A Critical Examination of Satellite Cloud Retrieval from AVHRR in the Arctic Using SHEBA Data

XIAOZHEN XIONG*

Geophysical Institute, University of Alaska Fairbanks, Fairbanks, Alaska

DAN LUBIN

Scripps Institution of Oceanography, University of California, San Diego, La Jolla, California

WEI LI AND KNUT STAMNES

Stevens Institute of Technology, Hoboken, New Jersey

(Manuscript received 10 December 2001, in final form 6 June 2002)

ABSTRACT

This study examines the validity and limitations associated with retrieval of cloud optical depth τ and effective droplet size r_e in the Arctic from Advanced Very High Resolution Radiometer (AVHRR) channels 2 (0.725–1.10 μm), 3 (3.55–3.93 μm), and 4 (10.3–11.3 μm). The error in r_e is found to be normally less than 10%, but the uncertainty in τ can be more than 50% for a 10% uncertainty in the satellite-measured radiance. Model simulations show that the satellite-retrieved cloud optical depth τ_{sat} is overestimated by up to 20% if the vertical cloud inhomogeneity is ignored and is underestimated by more than 50% if overlap of cirrus and liquid water clouds is ignored. Under partially cloudy conditions, τ_{sat} is larger than that derived from surface-measured downward solar irradiance (τ_{surf}) by 40%–130%, depending on cloud-cover fraction. Here, τ_{sat} derived from *NOAA-14* AVHRR data agrees well with τ_{surf} derived from surface measurements of solar irradiance at the Surface Heat Budget of the Arctic Ocean (SHEBA) ice camp in summer, but τ_{sat} is about 2.3 times τ_{surf} before the onset of snowmelt. This overestimate of τ_{sat} is mainly due to the high reflectivity in AVHRR channel 2 over snow/ice surfaces, the presence of partial cloud cover, and inaccurate representation of the scattering phase function for mixed-phase clouds.

1. Introduction

The effects of clouds still constitute one of the largest uncertainties in the study of climate change, and this is particularly true in the Arctic. Satellite remote sensing has proven useful for deriving some cloud properties, such as cloud fraction, optical depth, effective droplet size, and liquid water path on a global basis (e.g., Twomey and Cocks 1982, 1989; Foot 1988; Nakajima and King 1990; Nakajima et al. 1991; Han et al. 1994, 1999; Platnick and Valero 1995; Platnick et al. 2001). However, improved observations of these properties at high latitudes are necessary to further our understanding of the role of clouds in climate. The availability of more than 20 yr of Advanced Very High Resolution Radiometer (AVHRR) data covering the Arctic makes this particular satellite dataset valuable for the retrieval of cloud properties for climatological studies.

Many studies have been conducted to determine cloud optical depth τ and effective particle radius r_e from the reflected solar radiation in the visible and near-infrared (NIR) spectral range, but most of them were done over low-albedo surfaces (King 1987; Rossow et al. 1989; Nakajima and King 1990; Nakajima et al. 1991; Han et al. 1994). These algorithms rely on the fact that the reflectance of clouds in a nonabsorbing channel in the visible wavelength region is primarily a function of cloud optical depth, whereas the reflectance in a water-absorbing channel in the NIR is primarily a function of cloud droplet size. However, in the polar regions, the surface is covered by snow/ice most of the time throughout the year, and visible solar radiation in AVHRR channel 1 (0.58–0.68 μm) that is reflected by clouds over a bright snow/ice surface is not as sensitive to the cloud optical depth as over a dark surface. So, it is difficult to use AVHRR channel 1 for the retrieval of τ over snow/ice surfaces. The reflectance in channel 2 (0.725–

* Current affiliation: QSS Group, Inc., Camp Springs, Maryland.

Corresponding author address: Knut Stamnes, Light and Life Laboratory, Department of Physics and Engineering Physics, Castle Point on Hudson, Stevens Institute of Technology, Hoboken, NJ 07030.
E-mail: kstamnes@stevens-tech.edu

1.10 μm) is more sensitive to the cloud optical depth over snow/ice surfaces and has been used for the retrieval of cloud optical depth in the Arctic (e.g., Han et al. 1999).

Based on the retrieval algorithm developed in this paper, we examine the uncertainties of retrieved τ and r_e. The results are limited to AVHRR, but the method itself could be applied to other, similar satellite instruments. The sources of uncertainty in cloud retrieval include 1) the error in the radiance measured by the satellite sensor, 2) the simplification of the cloud as a single homogeneous layer, 3) the use of a plane-parallel radiative transfer model (RTM), and 4) the choice of surface condition, that is, albedo and temperature. Because there is a large variation in cloud properties in both the vertical and horizontal directions, and because in situ measurements of cloud properties coordinated with satellite retrievals are scarce, especially in the polar regions, validation studies of cloud retrieval in the polar regions are important. The cloud optical depth derived from this improved AVHRR retrieval algorithm will be compared with that derived from surface measurements during the Surface Heat Budget of the Arctic Ocean (SHEBA) project.

2. Method

a. Radiative transfer model

The radiative transfer model used here is based on the discrete ordinate method (Stamnes et al. 1988, 2000; Thomas and Stamnes 1999). The atmosphere is assumed to consist of multiple adjacent plane-parallel homogeneous layers in which the single-scattering albedo and the phase function are taken to be constant within each layer but may vary from layer to layer. Molecular scattering is computed from Rayleigh scattering theory (Penndorf 1957; Thomas and Stamnes 1999). The moderate-resolution transmittance model and code (MODTRAN) with 2-cm^{-1} spectral resolution is used to compute clear-sky optical-depth profiles for atmospheric absorbers such as water, methane, ozone, nitrous oxide, and carbon monoxide (H_2O, CH_4, O_3, N_2O, CO) and for carbon dioxide (CO_2) and aerosols. Because there is no better information, the MODTRAN tropospheric background aerosol model is frequently used in the Arctic because the volume extinction coefficient of Arctic haze is similar to that of the tropospheric aerosol in MODTRAN (Blanchet and List 1983; Han et al. 1999). A subarctic model atmosphere (McClatchey et al. 1971; Anderson et al. 1986) is employed, but the atmospheric temperature distribution and the water vapor profile are taken from in situ sounding data. The lower boundary is treated as follows: For snow-free conditions, the surface is treated as a Lambert reflector with an assigned albedo; under snow-covered conditions, an additional layer of snow is added at the bottom of the atmosphere to represent snow overlying tundra (or sea ice). Optical properties are adopted from Warren and Wiscombe (1980) for snow, from Hu and Stamnes (1993) for liquid water clouds, and from Fu and Liou (1993) for ice clouds.

We focus on the retrieval of water-cloud properties in this paper because the retrieval of ice clouds over snow/ice surfaces from AVHRR data is much more difficult, if not impossible. The main reasons are that (i) ice clouds often coexist with underlying liquid water clouds and (ii) there is low contrast in channel 2 between ice clouds and snow/ice surfaces.

b. Description of retrieval method

The reflectance in AVHRR channels 1 (R_1) and 2 (R_2) over water clouds increases with cloud optical depth and decreases with the effective cloud droplet radius. However, because of the low contrast in channel 1 between the cloud and the bright surface that results from multiple reflections between the cloud base and the underlying snow/ice surface, AVHRR channel 2 is more sensitive than channel 1 to cloud optical depth. Our model simulations show that over snow/ice surfaces the range of variation in R_2 is 2–3 times larger than in R_1 for the same range of cloud optical depth τ. Moreover, a large correction for Rayleigh scattering effects is required when the 0.66-μm channel is used to retrieve cloud optical thickness, as pointed out by Wang and King (1997). Therefore, channel 2 is preferable to channel 1 for the retrieval of cloud optical depth over snow/ice surfaces, as demonstrated by Han et al. (1999).

The brightness-temperature difference between AVHRR channels 3 and 4 is much larger over clouds than over snow/ice surfaces (Yamanouchi and Kawaguchi 1992). This difference is due to the increased reflectance of solar radiation by clouds. The reflectance in the AVHRR 3.75-μm channel (R_3) depends primarily on cloud droplet size. The smaller the effective droplet radius is, the larger R_3 is because the backscattering increases with decreasing droplet size. Reflectance R_3 increases with τ but ''saturates'' when the optical depth becomes sufficiently large, because the penetration depth of photons at wavelengths near 3.75 μm is limited to a shallow top layer of the cloud. So, for sufficiently thick clouds it is possible to use R_3 independently to retrieve the effective cloud droplet size over any underlying surface, but R_3 normally needs to be used together with R_1 or R_2 to derive τ and r_e simultaneously (e.g., Han et al. 1999). Except for very thin clouds with $\tau < 2$, for which there are multiple solutions over Lambert surfaces as pointed out by Nakajima and King (1990), the solutions are unique. Multiple solutions are not a problem even for $\tau < 2$, if one includes the snow surface as an additional scattering/absorbing layer at the bottom of the atmosphere (Han et al. 1999).

For a pair of reflectances in AVHRR channels 2 (R_2) and 3 (R_3), one point can be identified that corresponds to a unique value of r_e and τ over snow/ice surfaces.

However, it is difficult to derive R_3 accurately from the satellite-measured radiance in AVHRR channel 3 because it includes contributions from the thermal components emitted by the cloud and the atmosphere as well as that of the reflected solar radiation. The thermal component needs to be removed to determine the reflectance R_3 required for the retrieval of r_e. The method used in this paper is similar to that adopted by Han et al. (1994, 1999) based on radiative transfer modeling. The thermal radiation in channels 3 and 4 depends on cloud-top temperature T_c and surface temperature T_g, in addition to r_e and τ. Given r_e, τ, and T_g, we can use the brightness temperature in channel 4 (BT4) to derive T_c and then to derive the thermal radiation in channel 3. So, we will need channels 2, 3, and 4 to derive τ, r_e, and T_c simultaneously.

Based on the radiative transfer model described above, several lookup tables (not shown) are generated for the retrieval. Lookup table 1 gives the reflectance in channel 2 as a function of cloud τ and r_e for snow surfaces with several snow grain sizes or for Lambert surfaces with different albedo, respectively. Lookup table 2 is similar to lookup table 1 but is for the solar reflectance in channel 3. Lookup table 3 gives the thermal radiance in channel 3 as a function of surface temperature, cloud-top temperature, cloud τ, and r_e. Lookup table 4 provides the brightness temperature in channel 4 as a function of surface temperature, cloud-top temperature, cloud τ, and r_e. Because we use AVHRR channel 2 for the retrieval of cloud optical depth, it is obtained at a wavelength of 0.86 μm, the center of AVHRR channel 2. In these lookup tables, R_2 and R_3 are tabulated also as a function of solar zenith angle, viewing angle, and azimuthal angle. We use 10 solar zenith angles θ_0 ranging from 35° to 70° and 10 viewing angles θ ranging from 0° to 65°. To account for the variation in the reflectance with the relative azimuthal angle ϕ, we use 10 terms in a Fourier expansion of the top-of-the-atmosphere (TOA) reflectance with azimuthal angle to compute the reflectance at any required azimuthal angle. This method is more accurate than using interpolation in azimuth, as shown by Lubin and Weber (1995).

Instead of the radiance, we use the normalized reflectance in AVHRR channels 2 and 3 in our retrievals. The solar reflectance R_3 is

$$R_3 = \frac{(L_3 - \varepsilon_3) \int \phi_3(\lambda) B_\lambda(T)\, d\lambda}{\mu_0 F_{03}/\pi}, \qquad (1)$$

where L_3 is the measured radiance, $\phi_3(\lambda)$ is the sensor spectral response function, F_{03} is the extraterrestrial solar irradiance, and λ is the wavelength. The second term in the numerator of Eq. (1) represents the thermal radiation in channel 3, which can be computed from the Planck function B_λ, the cloud-top temperature, and the emissivity ε_3.

If the cloud is sufficiently thick (i.e., $\tau > 10$), the cloud-top brightness temperature is equal to BT4. Because the transmittance is negligible over optically thick clouds, $\varepsilon_3 = 1 - R_3$. Substituting it into Eq. (1) and using T = BT4, we have

$$R_3 = \frac{L_3 - \int \phi_3(\lambda) B_\lambda(\text{BT4})\, d\lambda}{\mu_0 F_{03}/\pi - \int \phi_3(\lambda) B_\lambda(\text{BT4})\, d\lambda}. \qquad (2)$$

This is an accurate computation of R_3 over thick clouds, and we use it as a ''first-guess'' value R_3^0 in our retrieval for thin clouds.

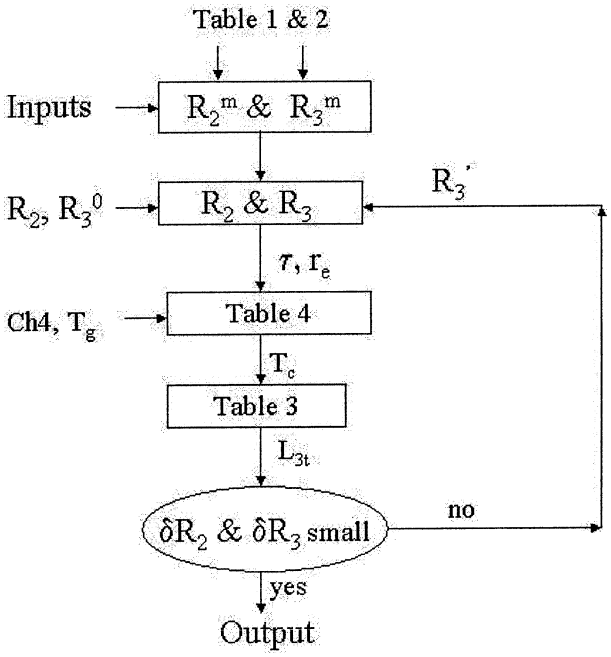

FIG. 1. Flowchart of the retrieval algorithm.

Our retrieval procedure is somewhat different from that of Han et al. (1999), as can be seen from a comparison of the flowchart (Fig. 1) with the corresponding flowchart provided by Han et al. (1999). The details of the retrieval procedure can be summarized as follows.

1) We interpolate the solar zenith angle, viewing angle, relative azimuthal angle, and surface albedo (or snow grain size) to derive the lookup tables of the TOA reflectances R_2^m and R_3^m. The superscript m is used to represent the model-simulated values.
   For a given sun–satellite geometry (solar zenith angle, viewing angle, and relative azimuthal angle) and surface condition, we use linear interpolation in the lookup tables to generate new and smaller tables of R_2^m and R_3^m that are only a function of cloud optical depth and effective droplet size. The surface is specified either in terms of its albedo or its snow grain size, retrieved from AVHRR channels 1 and 2 under clear-sky conditions. Surface temperature is derived

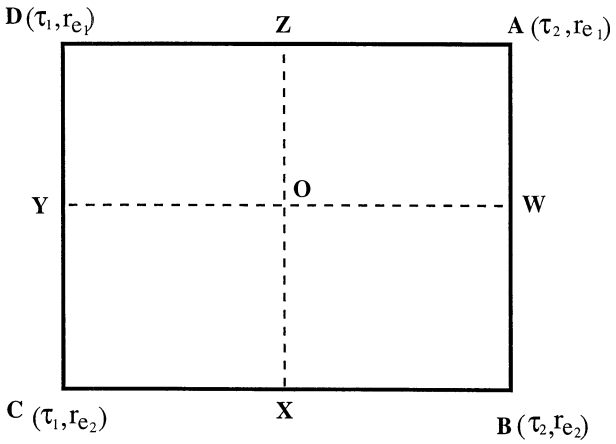

FIG. 2. Two-dimensional interpolation scheme to retrieve τ and r_e from lookup tables.

from clear-sky pixels using the algorithm of Key et al. (1997) in which T_g is represented as a function of brightness temperature in AVHRR channels 4 and 5.

2) We retrieve r_e and τ by searching the lookup tables R_2^m and R_3^m and doing two-dimensional interpolation to satellite-measured reflectance in channels 2 and 3. The interpolation scheme will be described below.
3) We retrieve the cloud-top temperature T_c from lookup table 4 using the retrieved r_e, τ, T_g, and BT4.
4) We use theory to estimate the thermal radiance in channel 3 L_{3t} from lookup table 3 using r_e, τ, T_c, and T_g. By replacing the second term in the numerator of Eq. (1) with L_{3t}, we can calculate a new value R_3' of the reflectance in channel 3. The theoretical value of the reflectance in channel 2, designated as R_2', corresponding to the retrieved τ and r_e, is estimated from the lookup table of R_2^m. If the following conditions are satisfied: $|R_2' - R_2^m| < 0.1\% \times R_2^m$ and $|R_3' - R_3^m| < 1\% \times R_3^m$, the retrieval is finished. Otherwise, we need to go back to step 2 to start another loop but with replacement of R_3 with R_3'.

Because we need to do an interpolation of τ and r_e in two dimensions until the theoretical values of R_2 and R_3 match those derived from the satellite measurements, we designed the following scheme to replace the iteration used by Han et al. (1999).

1) The lookup tables of channel 2 and channel 3 are searched to find the four closest points (in the box ABCD in Fig. 2) so that the satellite-measured R_2 and R_3 are located in this box, which is composed of R_2^m and R_3^m for two adjacent values of r_e and τ. In Fig. 2, τ increases from left to right, and r_e increases from top to bottom; that is, $\tau_1 < \tau_2$ and $r_{e1} < r_{e2}$, so both R_2^m and R_3^m have their maxima at point A (R_A) and their minima at point C (R_C), $R_C \le R_D \le R_A$, and $R_C \le R_B \le R_A$ (for simplicity, we do not mark channel numbers 2 and 3 here).
2) Interpolation is done to minimize the box by comparing the measured R_2 and R_3 with the value in the center of the box (R_O); W, X, Y, and Z are points at which the reflectance is the mean of the values at two pairs of adjacent points. Now, if $R_2 > R_O$ (similar for R_3), we will use box AWOZ; if $R_2 < R_O$, we use box OXCY; if $R_Z > R_2 > R_Y$, we use box ZOYD; otherwise we use box WBXO. In the same way we continue to minimize the box until it becomes as small as possible but with the measured R_2 and R_3 still inside this box. When no smaller box can be obtained, we interpolate to obtain $r_e^{(0)}$ and then obtain $\tau^{(0)}$ by interpolation within the array of $R_2[\tau, r_e^{(0)}]$.

With this scheme we can find unique solutions of τ and r_e quickly that correspond to a pair of reflectances in AVHRR channels 2 (R_2) and 3 (R_3). This is one of the advantages as compared with the iterative scheme used by Han et al. (1999). Also, in our retrieval scheme there are two separate tables for AVHRR channel 3 that correspond to the thermal radiation and the reflected solar radiation. As compared with Han et al. (1999) who used only one lookup table for both the thermal and the solar radiation components in channel 3, the size of our tables is small and allows for easy treatment of the variation of surface temperature and cloud-top temperature in the retrieval process.

3. Uncertainty analysis

The sources of uncertainty in the satellite retrieval of cloud properties mainly include 1) errors in satellite-measured radiance (i.e., measurement noise and calibration error); 2) errors related to the use of a homogeneous cloud layer in a plane-parallel radiative transfer model, such as (a) fractional cloud cover, (b) inhomogeneous cloud stratification, and (c) overlap of cirrus over low water clouds; and 3) the specification of the lower boundary conditions, that is, surface albedo and surface temperature. We will examine these uncertainties in cloud retrievals by comparing the retrieved τ and r_e with the values used as input to the RTM to simulate the ''satellite-measured'' radiance by forward model calculations.

a. Satellite measurements

Because there is no onboard calibration for AVHRR channels 1 and 2, uncertainties in the radiances measured by these solar backscatter channels, from sensor degradation, are a major challenge for their radiometric application. In general, the uncertainties are 5%–10%. As an example, the revised calibration of the *National Oceanic and Atmospheric Administration (NOAA)-14* AVHRR sensor by Rao and Chen (1999) yields radiance values that agree with those inferred from the previous calibration (Rao and Chen 1996) within 5% for about 900 days after launch (starting 30 December 1994) in

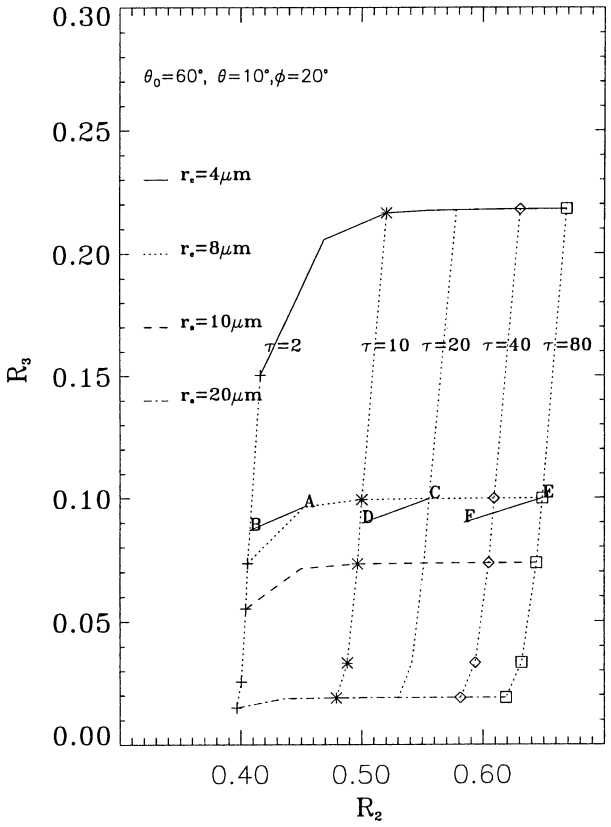

FIG. 3. Variation of R_2 vs R_3 for a variety of cloud optical depths and effective droplet sizes for the sun–satellite geometry of $\theta_0 = 60°$, $\theta = 10°$, and $\phi = 20°$ over snow surface. The surface snow grain size is fixed at 1000 μm. For a 10% decrease in R_2 and R_3, points ''A,'' ''C,'' and ''E'' change to points ''B,'' ''D,'' and ''F,'' respectively.

channel 1 and for about 500 days in channel 2. For a longer period, however, the calibration by Rao and Chen (1996) is inaccurate. The calibration coefficients of 1996 yield calibrated AVHRR reflectances obtained during the summer of 1998 that are overestimated by about 14% in channel 2 and about 8% in channel 1 as compared with the reflectances resulting from their revised 1999 calibration.

Figure 3 shows the reflectance in channels 2 and 3 as a function of cloud optical depth and effective radius over a snow surface. To illustrate the sensitivity of cloud retrieval to the uncertainty in satellite-measured radiances, let us examine the three points ''A'' (thin cloud), ''C'' (medium cloud), and ''E'' (thick cloud) in Fig. 3, which correspond to $r_e = 8$ μm and $\tau = 5$, 20, and 80, respectively. For a 10% decrease in R_2 and R_3, the points move to ''B,'' ''D,'' and ''F'' with $r_e = 9$ μm and $\tau = 2.2$, 10.3, and 32, respectively. The error in the retrieved r_e is about 10%, and the error in the retrieved τ is 50%–60%. Our simulations also show that the error is larger when retrieved from radiances in the forward- rather than in the backward-scattering direction. From this figure, we also note that if there is an error in R_3 only but R_2 is accurate, the error in the retrieved τ is small. Simple approximate analytic relationships of the sensitivity of τ and r_e versus the radiances in the visible and near infrared channels were obtained by Platnick et al. (2001).

b. Cloud fraction

Because the spatial resolution for AVHRR is at best 1.1 km (nadir), the pixel may be partly cloud covered. Identification of cloud fraction within a single AVHRR pixel has been accomplished over warm ocean surfaces (Coakley and Bretherton 1982) but needs validation for the Arctic. So, we need to test the effect of a misidentification of partly cloudy pixels as overcast on the retrieval of cloud optical depth and effective droplet radius and on the resulting uncertainty in the estimation of the radiation budget. For a partly cloudy pixel over a snow surface, the reflectance of channel 2 is assumed to be a linear function of cloud cover fraction that can be calculated as

$$R_2 = R_{2\text{cld}} f + R_{2\text{clr}}(1 - f), \tag{3}$$

where $R_{2\text{cld}}$ and $R_{2\text{clr}}$ are the TOA reflectances for overcast and clear conditions, respectively, and f is the cloud cover fraction. In a similar way, the reflectance in channel 3 is

$$R_3 = R_{3\text{cld}} f + R_{3\text{clr}}(1 - f) \sim R_{3\text{cld}} f, \tag{4}$$

where $R_{3\text{cld}}$ is the reflectance for overcast conditions and $R_{3\text{clr}}$ is the reflectance for clear conditions. Because the reflectance in AVHRR channel 3 is much larger over a cloud than over a cloud-free surface, $R_{3\text{clr}}$ is much less than $R_{3\text{cld}}$ and can be neglected.

When $f = 0.9$, R_3 is about 10% lower than under overcast conditions, and R_2 is about 5% lower than under overcast conditions for a snow surface, if we assume that $R_{2\text{clr}}$ over a snow surface is about 60% of $R_{2\text{cld}}$. Over a ''dark'' surface $R_{2\text{clr}}$ is much smaller than $R_{2\text{cld}}$, and so both R_3 and R_2 are about 10% lower than under overcast conditions when $f = 0.9$. Figure 4 shows the variation of retrieved cloud optical depth and the effective droplet radius for broken cloud cover with f varying between 0.25 and 1.0. Here, a water cloud with $r_e = 10$ μm and $\tau = 30$ is used, the sun–sensor geometry is $\theta_0 = 60°$, $\theta = 10°$, and $\phi = 50°$, and the surface snow grain size is 1000 μm. The errors in the retrieved cloud optical depth and effective droplet size for cloud-cover fractions of 0.5, 0.8, and 0.9 are summarized in Table 1. For a partly cloudy pixel with $f = 0.9$, the retrieved r_e is overestimated by about 10%, and the error in τ is about 9% for a medium cloud with $\tau = 15$ and 14% for a thick cloud with $\tau = 30$. Over a dark surface the error in τ will be larger than that over a snow/ice surface.

For partial cloud cover, the downward solar surface irradiance (DSSR) is often computed as follows:

$$\text{DSSR} = F_{\text{cld}} f + F_{\text{clr}}(1 - f), \tag{5}$$

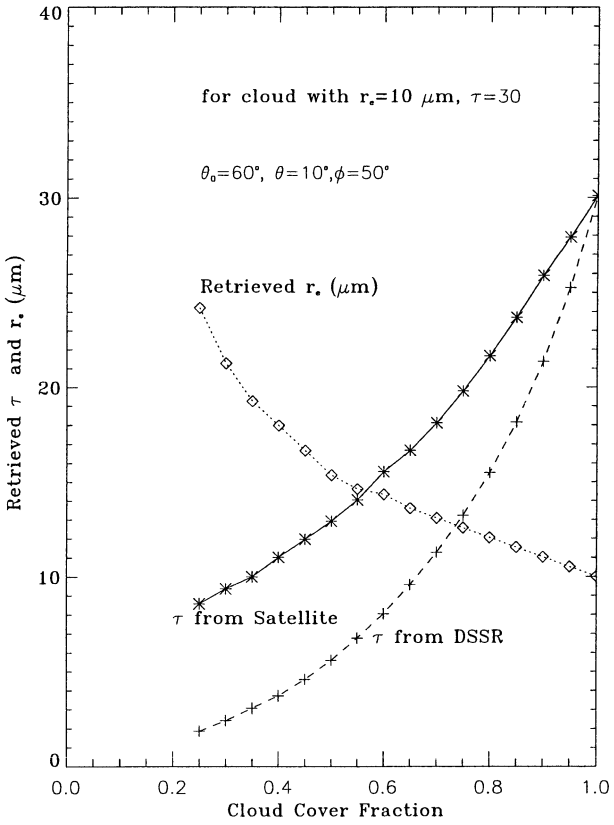

FIG. 4. Variation of the retrieved r_e and τ from satellite data as a function of cloud-cover fraction. The dashed line is the retrieved τ from DSSR; the solid line and dotted line are the retrieved τ and r_e from AVHRR, respectively. The cloud is assumed to consist of liquid water with $r_e = 10$ μm and $\tau = 30$. The sun–satellite geometry is given by $\theta_0 = 60°$, $\theta = 10°$, and $\phi = 50°$, and the surface snow grain size is fixed at 1000 μm.

where the downward irradiance is denoted by F_{cld} under overcast and by F_{clr} under clear-sky conditions. The limited spatial resolution of satellite sensors implies that it is difficult to obtain information about clouds at the subpixel level. In satellite retrievals, we either treat the pixel as cloudy or as clear and retrieve the cloud properties for cloudy pixels. These satellite-retrieved cloud optical depths and effective droplet sizes can be used as inputs to a 1D RTM, in which the cloud is taken to be a homogeneous layer, to compute the downward solar irradiance DSSR* for a partially cloudy pixel. Because the satellite-retrieved cloud τ for partly cloudy conditions is smaller than under overcast conditions while r_e is larger, and because the dependence of DSSR on cloud optical depth is nonlinear, DSSR* computed from the satellite-retrieved cloud τ is found to be smaller than DSSR computed from Eq. (5), based on our model simulations. The relative error between DSSR* and DSSR computed from Eq. (5) is shown in Fig. 5 for a cloud-cover fraction varying between 0.25 and 1.0. In this simulation, the solar zenith angle θ_0 was 60°, cloud $\tau = 15$, and $r_e = 10$ μm. Results for two surface conditions are shown. One is for a snow surface with snow grain size of 1000 μm, and the other is for a ''Lambertian'' surface with an albedo of 0.2. In Fig. 5, for partial cloud cover over a snow surface, DSSR* is smaller than DSSR by as much as 30%, and for a cloud-cover fraction of 0.8 the differences are about 13% and 15% for a snow surface and a low-albedo surface, respectively. These errors are larger for thick clouds; for example, when $\tau = 30$ and $f = 0.8$, the errors are about 18% and 21%, respectively. From Fig. 5 we note that this error is normally larger for low- than for high-albedo surfaces when the cloud-cover fraction is larger than 0.5.

TABLE 1. Retrieval error of cloud optical depth τ and cloud effective droplet size r_e (μm) for partial cloud cover.

f	$r_e = 10$ (μm)	$\tau = 15$	$\tau = 30$	$\tau = 30$ (DSSR)
0.5	15.4 (54%)	8.7 (42%)	12.9 (57%)	5.6 (81%)
0.8	12.1 (21%)	12.4 (17%)	21.7 (28%)	15.5 (48%)
0.9	11.0 (10%)	13.7 (9%)	25.9 (14%)	21.4 (29%)

The downward solar irradiance estimated from the

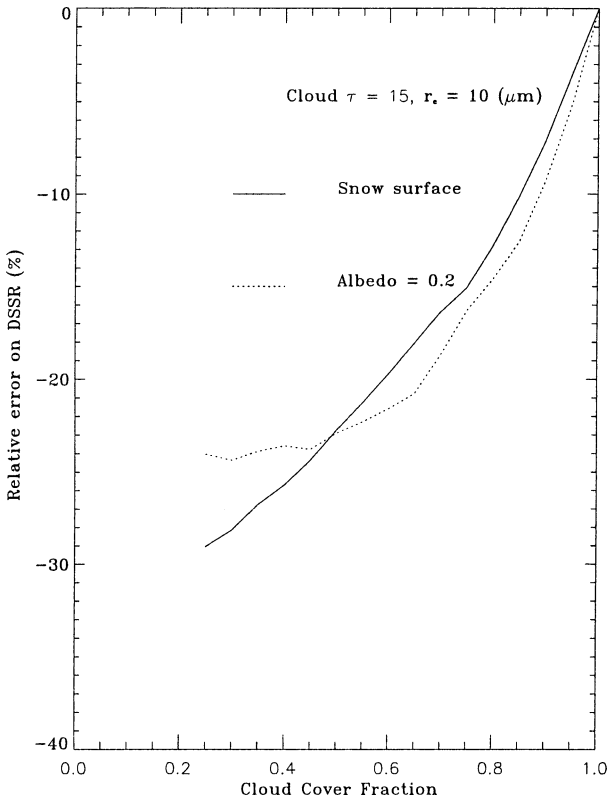

FIG. 5. Relative error in the computed downward irradiance DSSR* based on satellite-retrieved cloud optical depth and a homogeneous cloud layer, as compared with DSSR computed from the traditional method [Eq. (5)] for partial cloud cover. The solid line is over a snow surface with an snow grain size of 1000 μm, and the dotted line is over a Lambertian surface with an albedo of 0.2. The cloud is assumed to consist of liquid water with $r_e = 10$ μm and $\tau = 15$. The sun–satellite geometry was taken to be $\theta_0 = 60°$, $\theta = 10°$, and $\phi = 50°$.

satellite-derived cloud optical depth under partly cloudy conditions is smaller than that computed from Eq. (5); that is, $\mathrm{DSSR}^*(\tau_{\mathrm{sat}}) < \mathrm{DSSR}(\tau_{\mathrm{surf}})$. Thus, if we assume that DSSR obtained from Eq. (5) is accurate and use it to retrieve the cloud optical depth, this retrieved cloud optical depth τ_{surf} is expected to be smaller than the value τ_{sat} derived from satellite data; that is, $\tau_{\mathrm{sat}} > \tau_{\mathrm{surf}}$. Based on DSSR computed from Eq. (5) we retrieved the ''effective'' cloud optical depth τ_{surf} using the algorithm of Leontyeva and Stamnes (1994). This retrieved τ_{surf} is plotted in Fig. 4 as a function of cloud-cover fraction. Comparison of τ_{surf} and τ_{sat} (see Table 1) shows that for a cloud-cover fraction of 0.9, $\tau_{\mathrm{sat}} = 25.9$ and $\tau_{\mathrm{surf}} = 21.4$, whereas for $f = 0.5$, $\tau_{\mathrm{sat}} = 12.9$ and $\tau_{\mathrm{surf}} = 5.6$. So, for the same partial cloud cover, τ_{sat} is 1.3–2.3 times as large as τ_{surf}. From these simulations, we see that the presence of partial cloud cover might be an important reason for the overestimate of cloud optical depth derived from satellite measurements.

c. Cloud inhomogeneity in the vertical direction

Field observations show that terrestrial water clouds exhibit significant vertical inhomogeneity, with effective droplet radius increasing quasi-linearly from cloud bottom to cloud top except in the uppermost optically thin entrainment region (Tsay et al. 1989; Nakajima and King 1990; Olsson et al. 1998; Harrington et al. 1999). In situ measurements by Slingo et al. (1982), Stephens and Platt (1987), Albrecht et al. (1988), and Spinhirne et al. (1989) showed that the effective droplet radius at the bottom of the cloud is about 0.49–0.58 of its value at the cloud top. Nakajima and King (1990) showed that for clouds with $\tau \geq 8$, the effective droplet radius determined using the 0.75- and 2.16-μm channels is 85%–95% of the radius at the cloud top, which corresponds in turn to an optical depth (penetrated by photons) that is 20%–40% of the total optical thickness of the cloud layer. Remote sensing over marine stratocumulus and in situ measurements by Nakajima et al. (1991) showed that remote sensing retrievals tended to overestimate the effective radius by 2–3 μm and to overestimate optical thickness if it is small and to underestimate it if it is large.

To examine the effect of cloud vertical stratification on satellite remote sensing of cloud properties from AVHRR in the Arctic, a vertically inhomogeneous cloud stratification is considered by dividing the cloud into five layers with r_e increasing from cloud bottom to top according to the model of Stephens and Platt (1987). Figure 6 shows the computed reflectance R_2 (upper panel) and R_3 (lower panel) over a snow surface for cloud-top effective droplet radius $r_e = 5$ and 15 μm and different cloud optical depths. For comparison, the reflectances for a homogeneous cloud with r_e taken to be the same as the value at cloud top for the inhomogeneous cloud are also shown. Because the cloud reflectance is larger for smaller droplet size, R_2 and R_3 are higher for

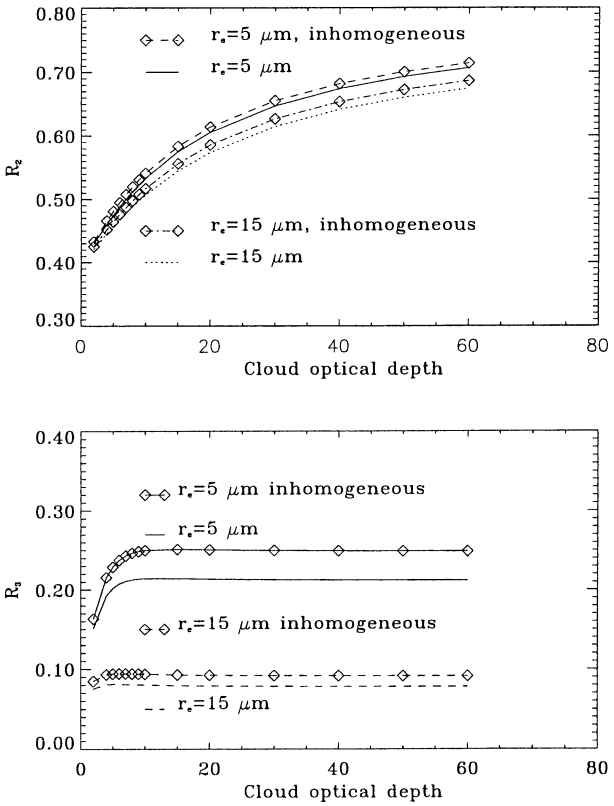

FIG. 6. Difference between (top) simulated R_2 and (bottom) R_3 as a function of τ and r_e for homogeneous and inhomogeneous water clouds when $\theta_0 = 50°$, $\theta = 10°$, and $\phi = 50°$, and the surface snow grain size is fixed at 1000 μm.

an inhomogeneous than for a homogeneous cloud with the same cloud top r_e. Because reflectance in channel 3 is very sensitive to effective droplet radius, R_3 is 15%–20% larger for an inhomogeneous cloud than for a homogeneous cloud with the same cloud-top effective droplet radius, whereas the difference in channel 2 is very small. Using these simulated reflectances as inputs to our cloud retrieval algorithm, as described before, we retrieved τ and r_e.

The upper panel of Fig. 7 shows the relative error of the derived cloud optical depth to the true optical depth as a function of r_e (top) for cloud $\tau = 4$, 15, and 30. These results demonstrate that the satellite-derived τ is overestimated by up to 20% and that the error is larger for clouds with a larger cloud effective droplet size. The lower panel of Fig. 7 shows the retrieved effective droplet radius in comparison with the value at cloud top as a function of τ for cloud top $r_e = 5$ and 15 μm in inhomogeneous clouds. The retrieved r_e is 10%–20% lower than the r_e at the top of the cloud. These retrieved r_e values are reasonable because the photons have a finite penetration depth and thus respond also to the smaller droplets below cloud top. The smaller the cloud effective droplet size is, the larger the relative error of the retrieved r_e is when compared with that at cloud

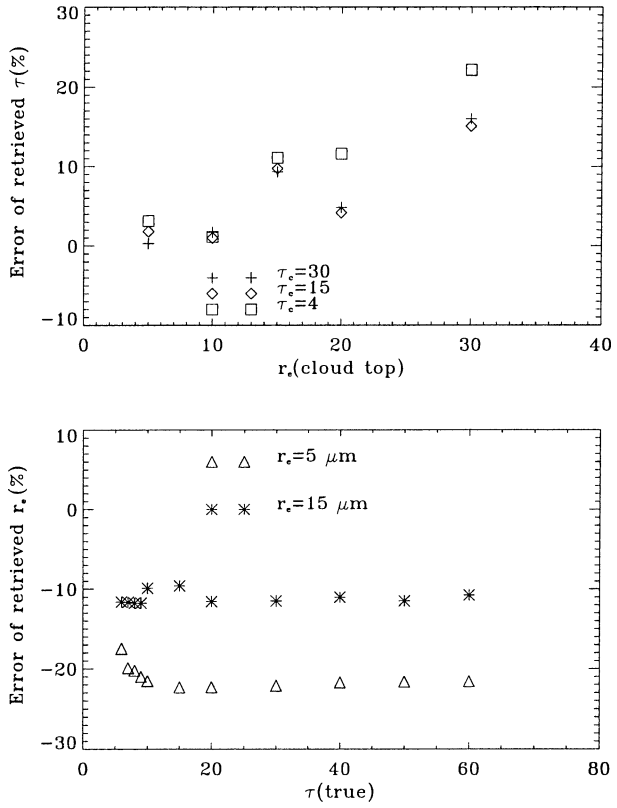

FIG. 7. Error in the (top) retrieved cloud optical depth and (bottom) retrieved effective radius as a function of τ and r_e at cloud top for vertically inhomogeneous clouds.

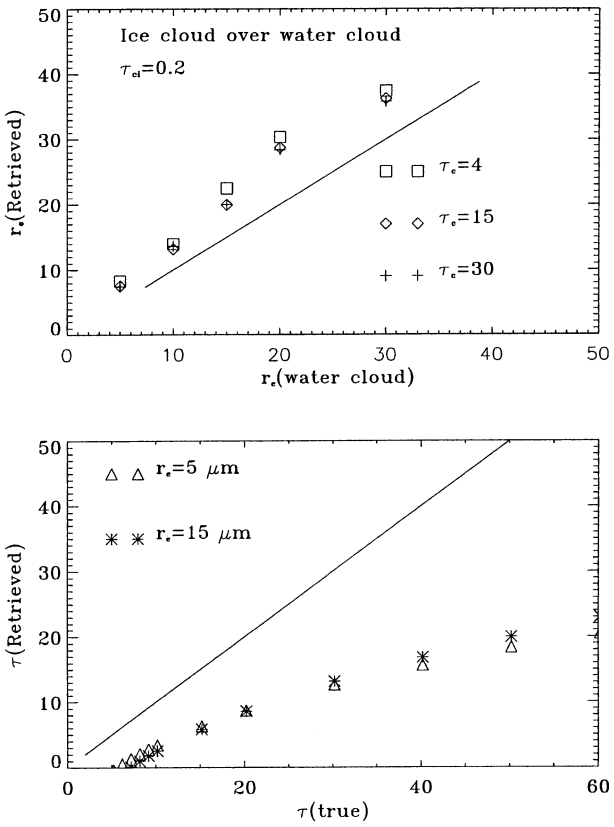

FIG. 8. Comparison between the (top) retrieved r_e and (bottom) τ and the true values for a liquid water cloud when a cirrus cloud located between 7 and 8 km overlies the liquid water cloud. The cirrus properties are held constant with $D_e = 60$ μm and $\tau_{ci} = 0.2$ (0.86 μm).

top. The ratio of the retrieved r_e to the effective droplet size at the cloud top strongly depends on the assumption made about the rate of increase of the cloud effective droplet size from cloud bottom to cloud top.

d. Overlap of cirrus over low water clouds

Summertime Arctic stratus clouds are believed to form as relatively warm and moist continental air flows over the pack ice, and radiative and diffusive cooling at the colder surface and longwave emission to space initiate the condensation (Herman and Goody 1976; Curry et al. 1988). These clouds are frequently observed to consist of multiple layers (e.g., Tsay and Jayaweera 1984; Curry et al. 2000), but the formation mechanisms are still not understood well although several have been proposed (Herman and Goody 1976; Tsay and Jayaweera 1984; Olsson et al. 1998; Harrington et al. 1999). The SHEBA surface lidar or radar observations and AVHRR observations indicate that multilayer clouds are a common feature in the Arctic (Curry et al. 2000).

To examine the effect of overlap of cirrus over liquid water clouds on the satellite retrieval of τ and r_e, we performed model simulations for a two-layer cloud system. The cirrus layer is assumed to be located between 7 and 8 km, to have a crystal diameter $D_e = 60$ μm, and to have an optical depth $\tau_{ci} = 0.2$. The liquid water cloud is assumed to be located between 1 and 2 km, and its cloud droplet effective radius and optical depth are allowed to vary. Reflectances in channels 2 and 3 for a variety of water cloud optical depths and effective radii are computed as inputs to the cloud retrieval algorithm (liquid water cloud). Comparison of the retrieved cloud optical depth and the droplet effective radius with the input water cloud τ and r_e is shown in Fig. 8. In the upper panel of Fig. 8, the retrieved effective droplet radius is larger than that of the input value by 35%–50%, whereas the retrieved cloud optical depth is underestimated by 70%–80%. This result is because the reflectances in channels 2 and 3 over ice clouds are much smaller than those over liquid water clouds.

e. Other sources of error

As mentioned in the previous section, the reflectance in channel 3 depends on the cloud optical depth but saturates when the cloud becomes sufficiently thick. Thus, when $\tau > 10$, the contribution of the surface reflection to the TOA radiance in channel 3 can be ne-

glected. However, the reflectance in channel 2 is sensitive to cloud optical depth even when $\tau > 50$. This fact implies that part of the solar radiation in this band is able to pass through thick clouds and reach the surface. Hence, the effect of surface reflection on the TOA radiance in channel 2 is large over snow/ice surfaces, and an error in the surface albedo will result in some error in the retrieved cloud optical depth. If the albedo is underestimated, the TOA reflectance predicted by the model will be underestimated. As shown in Han et al. (1999) for a tundra albedo of 0.06 with an uncertainty of 0.04, the error is less than 20% when $\tau > 3$, but the relative error can be as large as 60%–70% for $\tau = 1$. Over a snow surface, for an error of 10% in the snow grain size, the error in τ is less than 20%. Our model simulations show that over a Lambertian surface with albedo of 0.75, an error in albedo of 10% could result in an error in τ of 30%–50%.

Our model simulations show that if volcanic aerosols are included the simulated reflectance in channel 3 will be higher than in the absence of these aerosols. Thus, if volcanic aerosols are present in the stratosphere, the retrieved r_e for a given reflectance in channel 3 will be underestimated. Based on our analysis, this error in r_e can be as large as 10%–15% for a major volcanic eruption. In normal situations, the error will be smaller. The retrieved effective cloud droplet size tends to be smaller than it would be if volcanic aerosols were included in the model. Because data on volcanic aerosol optical properties are unavailable in the following cloud retrievals, volcanic aerosols are not included in the radiative transfer model.

Because we need to use the brightness temperature in channel 4 and the surface temperature to remove the thermal radiation in channel 3, an uncertainty in the surface temperature results in an uncertainty in the estimated thermal radiation in channel 3 for an optically thin cloud. This uncertainty influences the retrieval of effective droplet size r_e and cloud-top temperature T_c. Overestimation of the surface temperature will overestimate the thermal radiation emitted from the surface in channels 3 and 4. This result implies that T_c derived from channel 4 will be underestimated and will result in overestimation of the solar reflectance in channel 3, and thus the derived cloud droplet size may be underestimated.

The error in the retrieval method itself resulting from the interpolation or extrapolation in the lookup tables is relatively small. From our analysis, we found that the interpolation error is less than 1 in τ and is less than 0.5 μm in r_e, but it may be larger when $\tau < 2$ (Han et al. 1999; Nakajima and King 1990).

4. Case studies

a. Cloud effective droplet size and optical depth on 4 May 1998, SHEBA

In the SHEBA project the National Center for Atmospheric Research (NCAR) C-130 was used to ''map'' the surface and cloud characteristics on a horizontal scale up to 50 km × 50 km with a resolution of 10–100 m. This mapping was coordinated with satellite overpasses of *NOAA-12* and *-14* over the ice camp (Curry et al. 2000). The NCAR C-130 carried Particle Measuring Systems, Inc., cloud microphysical probes to measure the cloud droplet size distribution between 1.4 and 2250 μm in radius. One of these probes, the forward scattering spectrometer probe (FSSP), was used to measure the cloud droplet spectrum, mean particle diameter, and water/ice content.

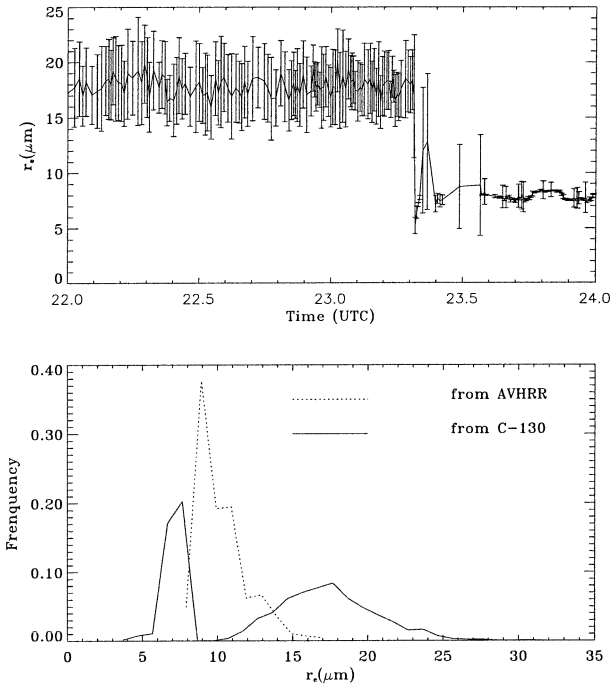

FIG. 9. (top) Variation of in situ effective cloud droplet size (for an average of 20 samples) measured by the FSSP deployed on the C-130 aircraft between 2200 and 2400 UTC on 4 May 1998. (bottom) Histograms of the effective cloud droplet size measured from the C-130 (solid line) and derived from the AVHRR overpass at 2250 UTC on 4 May 1998 (dotted line).

The upper panel of Fig. 9 shows the measured effective cloud droplet size between 2200 and 2400 UTC on 4 May 1998. Every point represents an average of measured r_e for 20 samples. Radar and lidar images show that a water droplet–dominated layer occurred between two ice crystal layers (Curry et al. 2000; Dong et al. 2001). The ice crystals from the dissipating altostratus fell through the liquid-phase cloud layer to the surface. The ceilometer-measured cloud-base height is about 0.6 km, and the radar-derived cloud-top height is near the top of the ice-crystal layer (4 km). A histogram of the effective cloud droplet size measured from the C-130 is shown in the lower panel of Fig. 9, from which the effective radius r_e exhibits two peaks: one at 7–8 μm and another one at about 17.5 μm. From the dependence of r_e on height (not shown), it is clear that the first peak corresponds to the liquid water cloud lo-

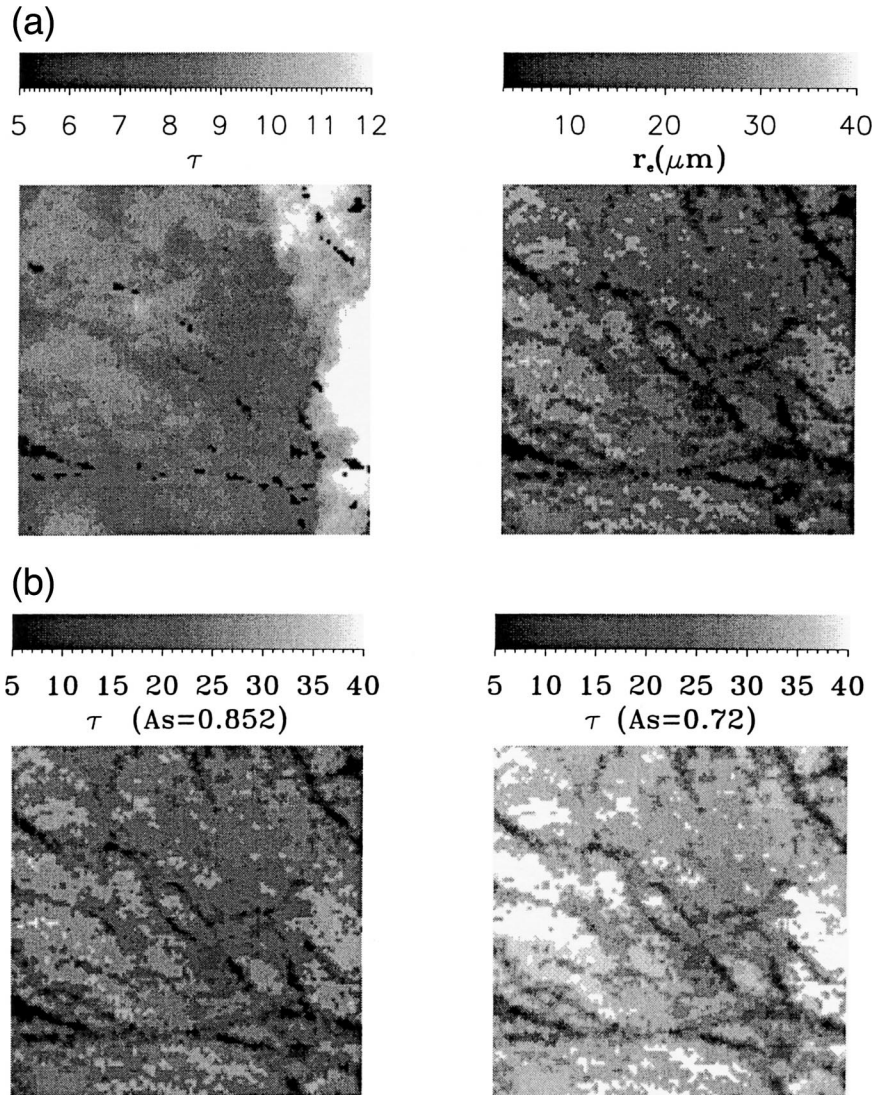

FIG. 10. (a) Satellite-retrieved (left) cloud effective droplet size r_e and (right) optical depth τ for a *NOAA-14* AVHRR overpass (100 km $\times$ 100 km) at 2250 UTC on 4 May 1998 over the SHEBA ice camp when the surface is treated as a snow layer. (b) Same as in (a) but for the satellite-retrieved cloud optical depth for a surface albedo of (left) $A_s = 0.852$ and (right) $A_s = 0.72$, respectively.

cated between the two ice-cloud layers, whereas the second peak corresponds to the ice cloud. From 2200 to 2400 UTC, the mean effective radius is 13.9 μm and the standard deviation is 5.6 μm. For comparison, the histogram of r_e derived from the AVHRR overpass at 2250 UTC on 4 May 1998 is also shown in the lower panel of Fig. 9. The mean effective radius is 8.8 μm and the standard deviation is 1.6 μm for the whole image.

An image of the satellite-derived effective droplet size is shown in the left panel of Fig. 10a. The size of the image is 100 $\times$ 100 pixels with a resolution of about 1.1 km, and the SHEBA ice camp is located in the center of the image. Most of the area in this image is covered by water clouds whose effective droplet sizes are 7–10 μm. The effective droplet size in this area is close to that in the first peak derived from the C-130 data, and the difference between them is about 10%. The area in the right 1/5 of the image represents clouds with effective droplet sizes larger than 12 μm, which size corresponds to the second peak in the C-130 observations. An accurate comparison of satellite-retrieved effective droplet size with in situ measurements obtained by instruments deployed on the C-130 aircraft should be based on pixels coordinated with the flight track of the C-130. Such work has been done, for example, by Nakajima et al. (1991). Some discussion of this case on 4 May 1998 can be found in Dong et al. (2001).

Here we will focus on the uncertainties in the retrieval of cloud optical depth. The right panel of Fig. 10a shows cloud optical depth derived from the algorithm described in the previous section. In our retrieval, AVHRR channels 1 and 2 are calibrated using the revised calibration of Rao and Chen (1999). Because the surface was covered by snow, we set the snow grain size at 200 μm and the mass fraction of soot at 0.02 ppmw so that the albedo over the snow surface from the model simulations is consistent with that from the measurements of Perovich et al. (1999). For most of the area in Fig. 10a, the cloud optical depth is about 20, with an average of 18.8. To compare the satellite-derived cloud optical depth with that derived from DSSR, we used 1-h averages of the downward solar irradiances measured during the overpass of the AVHRR sensor because the cloud optical depth τ derived from DSSR represents the accumulated effect of clouds over the spatial coverage of 20–30 km^2 above the ice camp. The algorithm of Leontyeva and Stamnes (1994) is used for this retrieval, and we obtained $\tau = 5.7$. In taking an average of satellite-measured radiance for 30×30 pixels over the SHEBA ice camp, the satellite-retrieved r_e is 9.7 μm, and τ is 16.2. Overall, the satellite-derived cloud optical depth tends to be larger than that derived from DSSR.

The overestimate of the optical depth by the AVHRR data was also demonstrated by Dong et al. (2001). Using *NOAA-14* AVHRR data taken at 2121 UTC 4 May 1998, Dong et al. used channels 1, 3, and 4, and the algorithms of Minnis et al. (1995) to derive $r_e = 9.5$ μm and $\tau = 56$, whereas the improved algorithm of Minnis et al. (1998) yielded $\tau = 26.7$. The difference between our results and those of Dong et al. (2001) may be due to use of different calibration, surface albedo, and retrieval algorithms. Using an albedo of $A_s = 0.72$, as adopted by Dong et al. (2001), in our algorithm, we retrieved the cloud optical depth shown in the right panel of Fig. 10b. The mean cloud optical depth τ retrieved is 32.3 for the whole image and is 29.7 for the center 30×30 pixels. These values are close to those obtained by Dong et al. (2001) based on the algorithm of Minnis et al. (1998). This result implies that the discrepancy caused by difference in calibration and retrieval method is small.

To demonstrate the effect of albedo on the retrieved τ, we show in Fig. 10b the retrieved τ for albedo $A_s = 0.852$ (left panel). The retrieved mean cloud optical depth τ is 21.2 for the whole image, and τ is 18.8 for the center 30×30 pixels. If the surface is assumed to be a layer of new snow with grain size of 200 μm, the retrieved τ values are 18.8 and 16.2, respectively. The differences in retrieved cloud droplet size for different values of surface albedo or snow grain size are less than 2%.

From these comparisons, we find that the retrieved optical depth depends strongly on the assumed surface condition. The lower the albedo is, the higher the retrieved cloud optical depth is. If the surface is assumed to be a layer of snow, a better result of retrieved τ can be achieved. So, our poor knowledge of snow surface reflectivity under cloudy conditions is one important source of uncertainty associated with the retrieval of cloud optical depth. For this reason, the use of a channel with smaller surface reflectivity would be better. Dong et al. (2001) used the along-track scanning radiometer (ATSR)-2 1.6-μm channel for a 10×10 pixel box centered at 175 km northwest of the ice camp to derive a cloud optical depth $\tau = 8.5$ and an effective droplet radius $r_e = 11.1$ μm, whereas the other two algorithms (Minnis et al. 1995, 1998) gave $r_e = 9.5$, $\tau = 57$ and $r_e = 9.5$, $\tau = 32.5$, respectively. The τ retrieved using the 1.6-μm ATSR-2 channel is clearly closer to that derived from ground-based DSSR.

b. *Comparison of cloud optical depth derived from AVHRR and from downward solar shortwave radiation*

To validate further the use of AVHRR data to retrieve cloud properties, we processed more than 100 overpasses of AVHRR data collocated with the SHEBA data during the melt season of 1998. SHEBA is a coordinated program aimed at addressing the interaction among surface energy balance, atmospheric radiation, and clouds over the Arctic Ocean by focusing on the key processes that determine ice albedo feedback in the Arctic pack ice. The Canadian Coastguard icebreaker *Des Groseilliers* was used as a floating station deployed in the Arctic Ocean at 75°16.3′N, 142°41.2′W and left to drift for a year. The SHEBA ice camp drifted considerably northwestward, and it was at 78.5°N, 166°W by the end of July of 1998. One full year of measurements were obtained at the ice camp from October of 1997 to October of 1998. These measurements include surface-based radiation measurements, atmospheric profiling by balloon-borne sounding systems, radar and lidar systems, and observations of clouds by several different instruments. The surface-based measured downward solar irradiances are used to derive the cloud optical depth using the algorithm of Leontyeva and Stamnes (1994). Similar to the approach of Leontyeva and Stamnes (1994) and Barker et al. (1998), we used 1-h averages of the downward solar irradiances measured during AVHRR overpasses when the solar zenith angle (SZA) was less than 70°. Among all available *NOAA-14* AVHRR overpasses during any particular day, we chose one or two of those closest to local noon that satisfied the condition SZA $< 70°$. Because no postlaunch calibration of AVHRR channels 1 and 2 is performed on *NOAA-12*, we used *NOAA-14* AVHRR data with 1.1-km pixel resolution for our retrieval. The revised postlaunch calibration by Rao and Chen (1999) is used. The spatial coverage used to retrieve cloud optical depth and effective droplet size is 30×30 pixels with the center over the SHEBA ice camp. The cloud optical depth and the effective droplet size for cloudy pixels are retrieved,

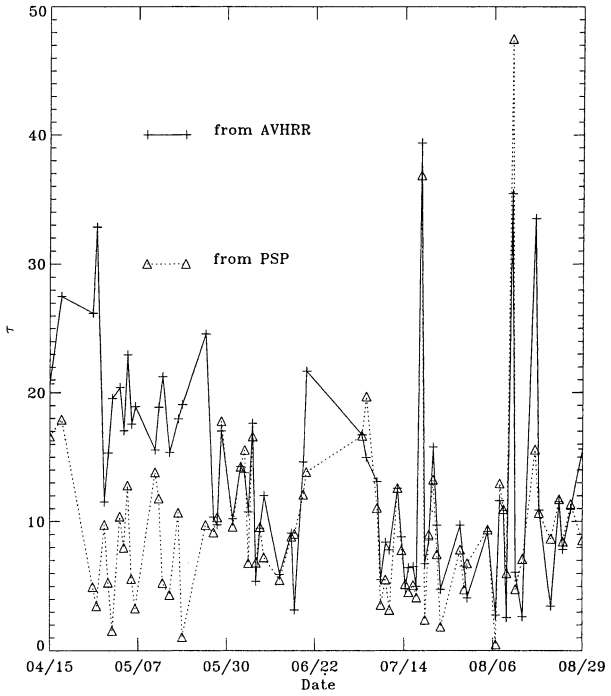

FIG. 11. Seasonal variation of cloud optical depth τ retrieved from AVHRR data (averaged over 30 × 30 pixels over SHEBA) over the central Arctic Ocean and its comparison with τ retrieved from downward solar irradiance measured by precision spectral pyranometers (PSP) over SHEBA (1-h average used).

and the average cloud optical depth is used for comparison with that derived from surface-measured solar irradiances. Selection of cloudy pixels is based on the cloud discrimination algorithm developed by Xiong (2000) in which a cloudy pixel is identified if the solar reflectance in channel 3 is higher than a certain threshold. Use of this algorithm with AVHRR daytime data between mid-April of 1998 and the end of August of 1998 yields AVHRR cloud-cover fractions consistent with SHEBA surface measurements with an error less than 10%.

The surface is taken to be new snow with snow grain size of 200 μm between 15 April and 19 May. Between 20 May and 9 June, we fix the snow grain size at 1000 μm. After 10 June, the surface is treated as a Lambertian reflector, and we adopt albedo values from the SHEBA measurements reported by Perovich et al. (1999). The satellite-retrieved cloud optical depth and the cloud optical depth retrieved from coordinated downward solar irradiances measured at SHEBA are shown in Fig. 11. This comparison shows that between 15 April and 30 May the satellite-retrieved mean cloud optical depth is $\tau_{sat} = 18.2$ while the surface-retrieved value is $\tau_{surf} = 8.0$. After 1 June, $\tau_{sat} = 10.0$ and $\tau_{surf} = 9.3$. If we only chose the images in which more than 60% of the pixels in the 30 × 30 pixel domain over the SHEBA ice camp are clouds that are thick enough and their optical depth and effective droplet sizes are successfully retrieved, the averaged τ_{sat} is 2.3 times τ_{surf} before the end of May; after 1 June, τ_{sat} is only 19.3% larger than τ_{surf}. The overestimate of τ_{sat} before June may be due to the fact that τ_{sat} represents an average τ value for successfully retrieved cloudy pixels, whereas τ_{surf} represents the average τ in a spatial domain of about 20–30 km^2 over the ice camp. This domain may include both cloudy and/or clear-sky conditions. To estimate the magnitude of this error, we used the average of the radiance for a domain of 30 × 30 pixels over the SHEBA ice camp for the retrieval. The retrieved τ_{sat} before 1 June is now 2.5 times τ_{surf}, and, after 1 June, τ_{sat} is 15.2% higher than τ_{surf}.

As shown in Fig. 11, the cloud optical depth derived from AVHRR is in better agreement with that derived from DSSR from June to August. As compared with summer, the cloud in the spring is thin and the cloud-cover fraction is generally smaller. Therefore, the possibility that the satellite-observed pixel consists of partial cloud cover in the spring may be much larger than in the summer. As discussed above, partial cloud cover will result in a higher τ_{sat} than τ_{surf}, and so the significant overestimate of τ_{sat} in the spring but not in the summer may be due to the presence of partial cloud cover; this contribution is about 50%–80%. Inaccurate representation of surface albedo and/or surface bidirectional reflectance distribution function (BRDF) is an important source of uncertainty. However, as discussed in the previous section, by treating the snow as an additional layer in the RTM, we retrieve a τ value closer to τ_{surf}. Another reason for this overestimate of τ_{sat} may be the higher probability that ice particles are present in clouds in spring than in summer, because we assumed that the clouds contained no ice particles. Incorrect representation of the scattering phase function for mixed-phased clouds and/or ice clouds is another source of uncertainty (Minnis et al. 1993).

5. Discussion

Estimation of cloud optical depth and effective radius is possible using AVHRR data in channels 2, 3 (3.75 μm), and 4. Over snow/ice surfaces, it is better to use AVHRR channel 2 than channel 1 for this retrieval. However, the high reflectivity over snow/ice surfaces in channel 2 implies that uncertainty in the surface albedo and/or surface BRDF may result in a large error in the retrieved τ. Treating the surface as a layer of snow in the RTM can decrease the error, but the proper choice of snow variables required to compute its optical properties accurately is not easy. A better way is to use a channel with a longer wavelength, such as the 1.6-μm channel (Dong et al. 2001).

Since the launch of *NOAA-15*, AVHRR makes use of a 1.6-μm channel instead of the 3.75-μm channel during daytime, so we lose information about the reflectance in the 3.75-μm channel. We may attempt using the 1.6-μm channel together with AVHRR channel 2 to retrieve

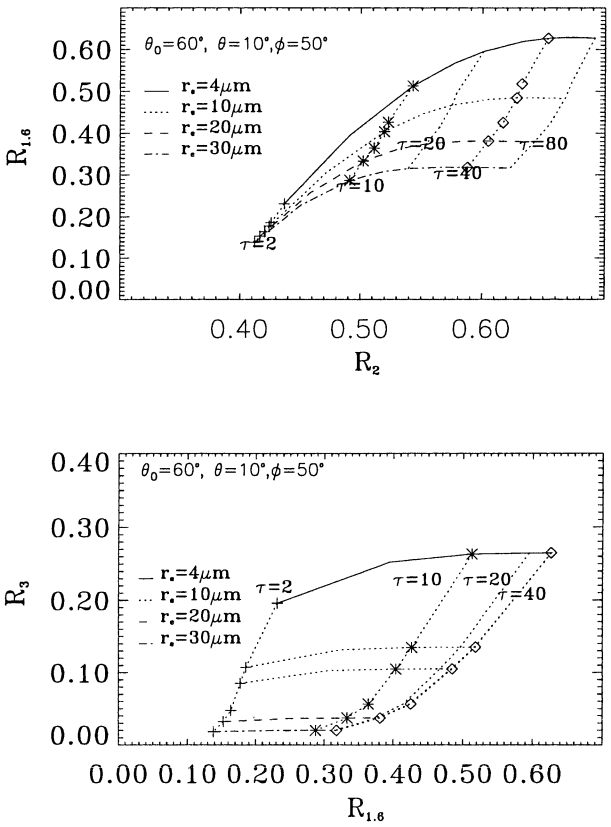

FIG. 12. (top) TOA reflectance in the 1.6-μm channel vs R_2 (0.86 μm) and (bottom) TOA reflectance in the 3.75-μm channel vs that in the 1.6-μm channel for a variety of cloud optical depths and effective droplet sizes when $\theta_0 = 60°$, $\theta = 10°$, and $\phi = 50°$.

τ and r_e, but the error in r_e is very large for clouds with $\tau < 10$, as shown in Fig. 12. Because the optical depth of clouds is about 10–15 during summer in the Arctic (Barker et al. 1998) and is a little smaller in the spring, it is difficult to use the 1.6-μm channel and AVHRR channel 2 on *NOAA-15* to retrieve effective droplet radius and optical depth simultaneously. However, use of the 1.6-μm channel, instead of a visible channel, and the 3.75-μm channel can produce more accurate values of τ and r_e over snow/ice surfaces for clouds if $\tau < 20$. The sensitivity of the TOA reflectance of clouds at 1.6 μm ($R_{1.6}$) with cloud optical depth decreases significantly when $\tau > 20$ (see lower panel of Fig. 12). So, simultaneous retrieval of r_e and τ may not be possible with an AVHRR sensor that switches channel 3 between 1.6 and 3.75 μm.

A (horizontally and vertically) homogeneous cloud layer embedded in plane-parallel RTMs constitutes the basis for most cloud retrieval algorithms. Because real clouds are inhomogeneous in both the vertical and horizontal directions (i.e., partial or broken cloud cover), there will be uncertainties in the retrieved cloud properties. These errors may lead to considerable uncertainties in estimated radiation budgets derived from satellite-retrieved cloud products, including optical depth and effective droplet size. For example, we use a simple linear model to compute the downward surface solar irradiance in the presence of broken clouds and to examine the uncertainties associated with partial cloud conditions. A better approach would be to use a rigorous three-dimensional RTM.

In our application of the retrieval algorithm to SHEBA data, we screened out the cirrus pixels in our assessment of error, but the pixels with cirrus over water clouds or multilayered clouds cannot be discriminated from AVHRR data. Partial cloudiness has not been removed in our retrievals because of the difficulty in the detection of partial cloud.

6. Summary and conclusions

Uncertainties associated with the retrieval of cloud properties in the Arctic from satellite remote sensing data are examined by use of model simulations of the atmospheric radiative transfer process over snow/ice surfaces and comparisons with surface-based observations obtained at the SHEBA ice camp. From these analyses we conclude the following points.

1) Errors in the satellite-measured radiance constitute one of the largest sources of uncertainty in cloud retrieval from space. A 10% error in the reflectance in AVHRR channel 2 (R_2) yields an uncertainty in the retrieved optical depth τ of about 50%–60%. The uncertainty in the retrieved effective cloud droplet size r_e is normally smaller than 10%. An overestimate of r_e results in a small overestimate of τ. For this reason, use of the calibration coefficients of Rao and Chen (1996) leads to a significant overestimation of τ. The revised calibration by Rao and Chen (1999) yields better results.
2) Penetration of photons in the 3.75-μm wavelength band is limited to a shallow layer near cloud top. Because the cloud droplet size typically decreases from cloud top to cloud bottom, this implies that the retrieved effective cloud droplet size, based on the assumption of a homogeneous cloud layer, is smaller than the droplet size at cloud top but larger than that at cloud bottom. This cloud inhomogeneity in the vertical direction will lead to an overestimation of τ of up to 20% and a retrieved effective cloud droplet size less than that at the cloud top by 10%–20%. Surface observations show that Arctic clouds often have two or three layers. The vertical stratification of single cloud layers, the multilayered structure, and the mixed-phase of clouds that are ignored in most retrieval algorithms have large influences on the cloud retrieval. The error in the satellite-derived τ can be more than 50% if the cloud pixels are contaminated by cirrus. However, from AVHRR data it is difficult to detect the multiple structure of clouds.
3) The cloud inhomogeneity in the horizontal direction,

that is, partial cloud cover, will result in an overestimate of r_e and an underestimate of τ. For a cloud-cover fraction of 0.9, r_e is overestimated by less than 10% and τ is lower than overcast conditions by about 10% over snow surfaces; over darker surfaces the error in τ will be larger. More important, for partly cloudy conditions, the AVHRR-derived cloud optical depth τ_{sat} is larger than that derived from surface measurements of irradiance (τ_{surf}) by 40%–130% for a cloud cover fraction from 0.5 to 0.9. A case study for 4 May, 1998 over the SHEBA ice camp shows that the AVHRR-derived effective droplet size is close to the value measured in situ by the FSSP deployed on the NCAR C-130 but that the AVHRR-derived cloud τ_{sat} is overestimated relative to τ_{surf}. From SHEBA data we found that before the onset of snowmelt τ_{sat} is about 2.3 times as large as τ_{surf}, but in the summer τ_{sat} and τ_{surf} agree well. The large overestimate of τ before the onset of snowmelt may be due to (a) ignoring partial cloud cover, (b) inaccurate treatment of surface reflectivity and/or surface BRDF over snow/ice surfaces, (c) ignoring cloud vertical inhomogeneity, and (d) inaccurate representation of the phase function for mixed-phase clouds.

4) For partly cloudy conditions, the downward solar surface irradiance derived from τ_{sat} is found to be underestimated by as much as 30%, depending on cloud-cover fraction. Cirrus overlying lower liquid water clouds can enhance the absorption of solar radiation in the atmospheric column significantly. Our investigation of partial cloud cover may appear to be an extreme representation of horizontally inhomogeneous clouds. Nevertheless, the resulting uncertainties in cloud retrievals and the differences between cloud optical depths derived from satellite data and from surface irradiance measurements give useful indications of the magnitude of the retrieval errors associated with our inability to treat horizontal cloud inhomogeneity lucidly. In view of the large uncertainties, this is a very important issue that needs to be considered when using satellite-derived cloud products.

Because τ_{surf} derived from surface measurements represents an average value integrated over an area of the sky of about 20–30 km^2, whereas τ_{sat} represents an average over just one pixel, determined by the spatial resolution of the AVHRR sensor, comparison of satellite cloud retrievals with in situ aircraft observations and surface-based remote sensing retrievals is problematic because the cloud may be inhomogeneous in both the vertical and horizontal directions. Further validations of the retrieval of cloud properties from AVHRR data should be undertaken to evaluate these uncertainties, and these validations should, if possible, be made for a homogeneous cloud covering at least 20–30 km^2 of the sky and for an extended homogeneous surface for which the surface albedo and/or the BRDF are accurately known.

The cloud inhomogeneity in vertical and horizontal directions results in an overestimate or underestimate of τ. Presence of cirrus over liquid water clouds results in an underestimate of τ. Because discrimination of cloud from snow/ice surfaces is much more difficult than from low-albedo surfaces, improvement of the cloud mask in the polar regions is necessary to improve cloud retrievals. With the deployment of new sensors, such as the moderate-resolution imaging spectroradiometer (MODIS) on the National Aeronautics and Space Administration *Terra* and *Aqua* satellites and the global imager (GLI) on the Advanced Earth Observing Satellite-II (ADEOS-II), many additional channels become available. Use of these new channels will enable us to improve both the cloud discrimination and the retrieval of cloud optical depth in the Arctic. The uncertainties in the retrieved τ are large. Hence, further validation of cloud retrieval in the Arctic is necessary to test the use of other channels (available on instruments such as MODIS and GLI) in order to assess retrieval capabilities and uncertainties in the presence of mixed-phase clouds, which are common in the Arctic. Data obtained from long-term measurements programs such as the Atmospheric Radiation Measurement (ARM) Program deployed on the North Slope of Alaska (Stamnes et al. 2000) provide an opportunity to assess the validity of retrievals based on these new instruments because several ground-based instruments, including lidar and radar in addition to state-of-the-art shortwave and longwave radiometers, are available for cloud and radiation observations. Data from these instruments are expected to be very useful for validation purposes.

Acknowledgments. Data were obtained from the ARM Program sponsored by the U.S. Department of Energy, Office of Science, Office of Biological and Environmental Research, Environmental Sciences Division. This research was supported by the National Science Foundation Office of Polar Programs under NSF OPP 9701840 and by the ARM Program.

REFERENCES

Albrecht, B. A., D. A. Randall, and S. Nicholls, 1988: Observation of marine stratocumulus clouds during FIRE. *Bull. Amer. Meteor. Soc.,* **69,** 618–626.

Anderson, G. P., S. A. Clough, F. X. Kneizys, J. H. Chetwynd, and E. P. Shettle, 1986: AFGL atmospheric constituent profiles (0–120 km). Hanscom Air Force Base Tech. Rep. AFGL-TR-86-0110 (OPI).

Barker, H. W., T. J. Curtis, E. Leontyeva, and K. Stamnes, 1998: Optical depth of overcast cloud across Canada: Estimates based on surface pyranometer and satellite measurements. *J. Climate,* **11,** 2980–2994.

Blanchet, J., and R. List, 1983: Estimation of optical properties of Arctic haze using a numerical model. *Atmos.–Ocean,* **21,** 444–465.

Coakley, J. A., Jr., and F. P. Bretherton, 1982: Cloud cover from high resolution scanner data: Detecting and allowing for partially filled fields of view. *J. Geophys. Res.,* **87,** 4917–4932.

Curry, J. A., E. E. Ebert, and G. F. Herman, 1988: Mean and turbulent structure on the summertime Arctic cloudy boundary layer. *Quart. J. Roy. Meteor. Soc.,* **114,** 715–746.

——, and Coauthors, 2000: FIRE Arctic Clouds Experiment. *Bull. Amer. Meteor. Soc.,* **81,** 5–29.
Dong, X., G. G. Mace, P. Minnis, and D. F. Young, 2001: Arctic stratus cloud properties and their effects on the surface radiation budget: Selected cases from FIRE ACE. *J. Geophys. Res.,* **106,** 15 297–15 312.
Foot, J. S., 1988: Some observations of the optical properties of clouds. I: Stratocumulus. *Quart. J. Roy. Meteor. Soc.,* **114,** 129–144.
Fu, Q., and K. N. Liou, 1993: Parameterization of the radiative properties of cirrus clouds. *J. Atmos. Sci.,* **50,** 2009–2025.
Han, Q., W. B. Rossow, and A. A. Lacis, 1994: Near-global survey of effective droplet radii in liquid water clouds using ISCCP data. *J. Climate,* **7,** 465–497.
Han, W., K. Stamnes, and D. Lubin, 1999: Retrieval of surface and cloud properties in the Arctic from NOAA AVHRR measurements. *J. Appl. Meteor.,* **38,** 989–1012.
Harrington, J. Y., T. Reisin, W. R. Cotton, and S. M. Kreidenweis, 1999: Cloud resolving simulations of Arctic stratus. Part II: Transition-season clouds. *Atmos. Res.,* **51,** 45–75.
Herman, G., and R. Goody, 1976: Formation and persistence of summertime Arctic stratus clouds. *J. Atmos. Sci.,* **33,** 1537–1553.
Hu, Y. X., and K. Stamnes, 1993: An accurate parameterization of the radiative properties of water clouds suitable for use in climate models. *J. Climate,* **6,** 728–742.
Key, J. R., J. B. Collins, C. Fowler, and R. S. Stone, 1997: High-latitude surface temperature estimates from thermal satellite data. *Remote Sens. Environ.,* **61,** 302–309.
King, M. D., 1987: Determination of the scaled optical thickness of clouds from reflected solar radiation measurements. *J. Atmos. Sci.,* **44,** 1734–1751.
Leontyeva, E., and K. Stamnes, 1994: Estimate of cloud optical thickness from ground-based measurements of incoming solar radiation in the Arctic. *J. Climate,* **7,** 566–578.
Lubin, D., and P. J. Weber, 1995: The use of cloud reflectance functions with satellite data for surface radiation budget estimation. *J. Appl. Meteor.,* **34,** 1333–1347.
McClatchey, R. A., R. W. Fenn, J. E. A. Selby, F. E. Volz, and J. S. Garing, 1971: Optical properties of the atmosphere. Air Force Cambridge Rep. AFCRL-71-0279, 85 pp.
Minnis, P., P. W. Heck, and D. F. Young, 1993: Inference of cirrus cloud properties using satellite-observed visible and infrared radiances. Part II: Verification of theoretical cirrus radiative properties. *J. Atmos. Sci.,* **50,** 1305–1322.
——, W. L. Smith Jr., D. P. Garber, J. K. Ayers, and D. R. Doelling, 1995: Cloud properties derived from *GOES-7* for the spring 1994 ARM Intensive Observing Period using version 1.0.0 of the ARM satellite data analysis program. NASA Rep. 1366, 59 pp.
——, D. P. Garber, D. F. Young, R. F. Arduini, and Y. Takano, 1998: Parameterizations of reflectance and effective emittance for satellite remote sensing of cloud properties. *J. Atmos. Sci.,* **55,** 3313–3339.
Nakajima, T., and M. D. King, 1990: Determination of the optical thickness and effective particle radius of clouds from reflected solar radiation measurements. Part I: Theory. *J. Atmos. Sci.,* **47,** 1878–1893.
——, ——, J. D. Spinhirne, and L. F. Radke, 1991: Determination of the optical thickness and effective particle radius of clouds from reflected solar radiation measurements. Part II: Marine stratocumulus observations. *J. Atmos. Sci.,* **48,** 728–750.
Olsson, P. Q., J. Y. Harrington, G. Feingold, W. R. Cotton, S. M. Kreidenweis, 1998: Exploratory cloud-resolving simulations of boundary-layer Arctic stratus clouds. Part I: Warm-season clouds. *Atmos. Res.,* **47–48,** 573–597.
Penndorf, R., 1957: Tables of the refractive index for standard air and the Rayleigh scattering coefficient for the spectral region between 0.2–20 μm and their application to atmospheric optics. *J. Opt. Soc. Amer.,* **47,** 176–182.
Perovich, D. K., and Coauthors, 1999: *SHEBA: Snow and Ice Studies.* CD-ROM. [Available from D. Perovich, CRREL, 72 Lyme Road, Hanover, NH 03755.]
Platnick, S., and F. P. J. Valero, 1995: A validation of a satellite cloud retrieval during ASTEX. *J. Atmos. Sci.,* **52,** 2985–3001.
——, J. Y. Li, M. D. King, H. Gerber, and P. Hobbs, 2001: A solar reflectance method for retrieving the optical thickness and droplet size and liquid water clouds over snow and ice surfaces. *J. Geophys. Res.,* **106,** 15 185–15 199.
Rao, C. R. N., and J. Chen, 1996: Post-launch calibration of the visible and near-infrared channels of the Advanced Very High Resolution Radiometer on the *NOAA-14* spacecraft. *Int. J. Remote Sens.,* **17,** 2743–2747.
——, and ——, 1999: Revised post-launch calibration of the visible and near-infrared channels of the Advanced Very High Resolution Radiometer (AVHRR) on the *NOAA-14* spacecraft. *Int. J. Remote Sens.,* **20,** 3485–3491.
Rossow, W. B., L. C. Gardner, and A. A. Lacis, 1989: Global seasonal cloud variations from satellite radiation measurements. Part I: Sensitivity of analysis. *J. Climate,* **2,** 419–458.
Slingo, A., S. Nicholls, and J. Schmetz, 1982: Aircraft observations of marine stratocumulus during JASIN. *Quart. J. Roy. Meteor. Soc.,* **108,** 833–856.
Spinhirne, J. D., R. Boers, and W. D. Hart, 1989: Cloud top liquid water from lidar observations of marine stratocumulus. *J. Appl. Meteor.,* **28,** 81–90.
Stamnes, K., S. C. Tsay, W. Wiscombe, and K. Jayaweera, 1988: Numerically stable algorithm for discrete-ordinate-method radiative transfer in multiple scattering and emitting layered media. *Appl. Opt.,* **27,** 2502–2509.
——, S.-C. Tsay, W. J. Wiscombe, and I. Laszlo, cited 2000: DISORT: A general-purpose Fortran program for discrete-ordinate-method radiative transfer in scattering and emitting layered media: Documentation of methodology. [Available online at ftp://climate.gsfc.nasa.gov/pub/wiscombe/Multiple_Scatt/.]
Stephens, G. L., and C. M. R. Platt, 1987: Aircraft observations of the radiative and microphysical properties of stratocumulus and cumulus clouds fields. *J. Appl. Meteor.,* **26,** 1243–1269.
Thomas, G. E., and K. Stamnes, 1999: *Radiative Transfer in the Atmosphere and Ocean.* Cambridge University Press, 517 pp.
Tsay, S. C., and K. Jayaweera, 1984: Physical characteristics of Arctic stratus clouds. *J. Appl. Meteor.,* **23,** 584–596.
——, K. Stamnes, and K. Jayaweera, 1989: Radiative energy budget in the cloudy and hazy Arctic. *J. Atmos. Sci.,* **46,** 1002–1017.
Twomey, S., and T. Cocks, 1982: Spectral reflectance of clouds in the near-infrared: Comparison of measurements and calculations. *J. Meteor. Soc. Japan,* **60,** 583–592.
——, and ——, 1989: Remote sensing of cloud parameters from spectral reflectance in the near-infrared. *Beitr. Phys. Atmos.,* **62,** 172–179.
Wang, M., and W. D. King, 1997: Correction of Rayleigh scattering effects in cloud optical thickness retrievals. *J. Geophys. Res.,* **102,** 25 915–25 926.
Warren, S. G., and W. J. Wiscombe, 1980: A model for the spectral albedo of snow. II. Snow containing atmospheric aerosols. *J. Atmos. Sci.,* **37,** 2734–2745.
Xiong, X., 2000: Cloud and surface properties and the solar radiation budget derived from satellite data over the Arctic Ocean: Comparisons with surface measurements and in situ aircraft data. Ph.D thesis, University of Alaska, Fairbanks, 217 pp.
Yamanouchi, T., and S. Kawaguchi, 1992: Cloud distribution in the Antarctic from AVHRR data and radiation measurements at the surface. *Int. J. Remote Sens.,* **13,** 111–127.